ARMA 12-422

Identifying Unstable Failure in Brittle Rock using the Finite Difference Method

Garvey, R.
Colorado School of Mines, Golden, CO, USA
Ozbay, M.U.
Colorado School of Mines, Golden, CO, USA

This paper was prepared for presentation at the 46th US Rock Mechanics / Geomechanics Symposium held in Chicago, IL, USA, 24-27 June 2012.

ABSTRACT:

A series of uniaxial and triaxial compressive strength tests were simulated using the explicit finite difference software FLAC3D to simulate and identify unstable failure in rock. A slender cylindrical specimen was calibrated using the Mohr-Coulomb strain-hardening/-softening constitutive model to behave as a weak, brittle coal. Instability was induced within the specimen through a relatively soft compressive loading system with an applied elastic response. Unbalanced forces, accelerations, velocities, and shear strain rates were recorded during the FLAC3D simulations and were all found to have a strong positive correlation with other indications of unstable failure. The use of numerical identifiers of unstable failure was shown to provide a potential method for detecting instability within an explicit finite difference model at a higher resolution than existing methods.

1. INTRODUCTION

Rockbursts and coal bumps occur in underground hard rock and coal mines when a volume of brittle rock is stressed beyond its strength by a comparatively soft loading system [1, 2]. This instability is accompanied by a transfer of stored potential energy from the loading system into the failing volume of brittle rock until a static equilibrium is reached within the entire system. The large magnitudes of energy released during unstable failures result in the rapid ejection of rock and debris into the working areas of the mine and pose a serious hazard to the safety of mining personnel [3]. Mitigating the effects of unstable failures is difficult in practice due to the complexities of measuring and predicting the complex interactions between in situ ground conditions and a volume of rock failing unstably. The speed of failure and the substantial damage which typically results has further restricted the amount of information which may be gained about dynamic phenomenon in large underground structures.

Numerical models are capable of addressing many of these practical concerns of studying and predicting instability in rock [4, 5]. The explicit finite difference software FLAC3D [6] has been shown in a previous study to be able to simulate unstable failure in a slender rock specimen during a uniaxial compressive strength test [7]. The results of this study have been extended to include more precise methods for identifying unstable failure in the continuum model through an analysis of the dynamic response of the gridpoints within the simulated specimen.

In FLAC3D, unstable failure conditions were found to result in large unbalanced forces acting at the gridpoints of the unstable volume of rock. The magnitude of these forces was proportional to the degree of instability, with little to no change observed between the stable failure cases. This analysis of unbalanced forces was extended to include additional measurements of accelerations, velocities, and shear strain rates to allow for multiple methods of detecting unstable equilibria in the model. These identifiers of unstable failure were applied to the analysis in order to increase the effective resolution for detecting instability within the controlled tests.

2. UNIAXIAL COMPRESSIVE STRENGTH TESTS

A series of uniaxial compressive strength tests were performed using FLAC3D while recording potential instability identifiers at the gridpoints and zones of the coal specimen. These identifiers consisted of unbalanced

forces, accelerations, and velocities at the gridpoints. The zone-level identifiers were shear strain rate and plastic shear strain rate. The maximum value of each identifier was recorded for all gridpoints and zones within the coal specimen.

A cylindrical coal specimen sized 1 m in diameter and 2 m in height was tested between two elastic platens each measuring 1 m in height. The combined system of platens and specimen is shown in Figure 1.

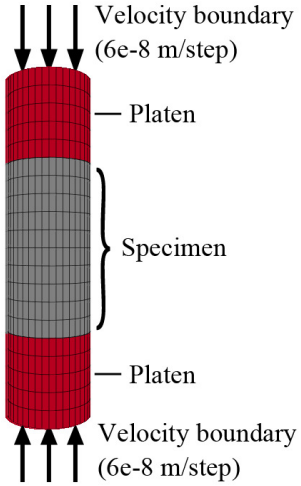

Fig. 1. Uniaxial compressive strength test configuration in FLAC3D model.

The elastic modulus of the platens was controlled between tests and spanned the range of 2 to 100 GPa. The coal specimen was calibrated using the Mohr-Coulomb strain-hardening/-softening (MCSS) constitutive law with the values provided from [7]. A mesh identical to that found in the preliminary study was used for these continued tests. Gridpoints were spaced at 0.2m intervals in the vertical and the outward radial directions. A calibration procedure had been employed for the given zone sizes in the previous study to achieve compressive strength behaviors approximate to those of coal. The specimen was calibrated to exhibit a peak strength of 7.9 MPa and a Young's modulus of 4.1 GPa. The specimen assumed a brittle failure response with a maximum post-peak drop of approximately -20 GPa.

A velocity boundary with a small rate of 6e-8 m/step was applied at the end of the platens to apply an increasing load onto the system until a specimen strain of 0.003 was achieved. At this point, the simulation was run for an additional 1000 steps and the system was allowed to come to static equilibrium.

The model was run in static solution mode with masses scaled artificially at the gridpoints. The ideal method for analyzing dynamic failure would be through a truly dynamic analysis, however uncertainties in the calibration of such a model and the length of time required to compute a dynamic solution made the static mode a more favorable option. The drawback of the static solution mode is that any measurements that are dependent on a time response hold little physical significance. Insight may still be gained by comparing a known stable failure case against an unknown, potentially unstable failure case. In this manner a measure of relative instability may be established.

A series of identical uniaxial compressive strength tests were run in which the coal specimen was represented using a plastic Mohr-Coulomb (MC) constitutive model. These tests provided insight into how loading system stiffness may directly affect the selected identifiers within the finite difference model. The specimen was calibrated to undergo plastic flow at a comparable stress value as the peak strength of the Mohr-Coulomb strain-softening (MCSS) model. The stable stress-strain response for the MCSS model is shown in Figure 2 along with the Mohr-Coulomb (MC) plastic model response as a comparison.

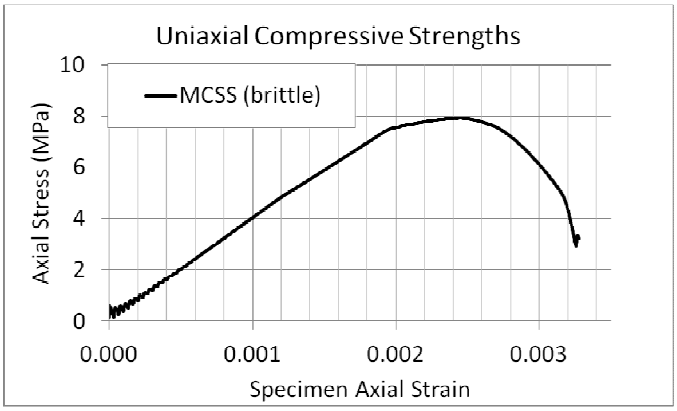

Fig. 2. Specimen stress-strain response of Mohr-Coulomb Strain-Hardening/-Softening (MCSS) and Mohr-Coulomb (MC) models.

2.1. Indications of Unstable Failure

Axial stresses were calculated during the test from the sum of the applied boundary forces divided by the cross-sectional area of the specimen. Strains were then recorded from the displacements at the specimen-platen contacts. The stress-strain responses of the specimens were calculated from these values and their post-peak responses were recorded. For the platens with an elastic moduli ranging from approximately 16 to 100 GPa, the post-peak stress-strain response of the specimen was consistent between UCS tests. However, for lower elastic platen moduli, unstable failure conditions were initiated and the specimen assumed a post-peak response identical to that of the elastic behavior of the loading system. This is demonstrated for the stable 40 GPa and unstable 2 GPa loading cases shown in Figure 3. The specimen in the unstable failure case assumed a -2 GPa post-peak stress-strain response which was identical to the elastic modulus of the loading system. For the platen Young's moduli lower than 16 GPa, the unstable loading

conditions were coupled with a dramatic increase in the maximum unbalanced force acting within the model. The second plot of Figure 3 compares the response of the maximum unbalanced force between the unstable and stable loading conditions.

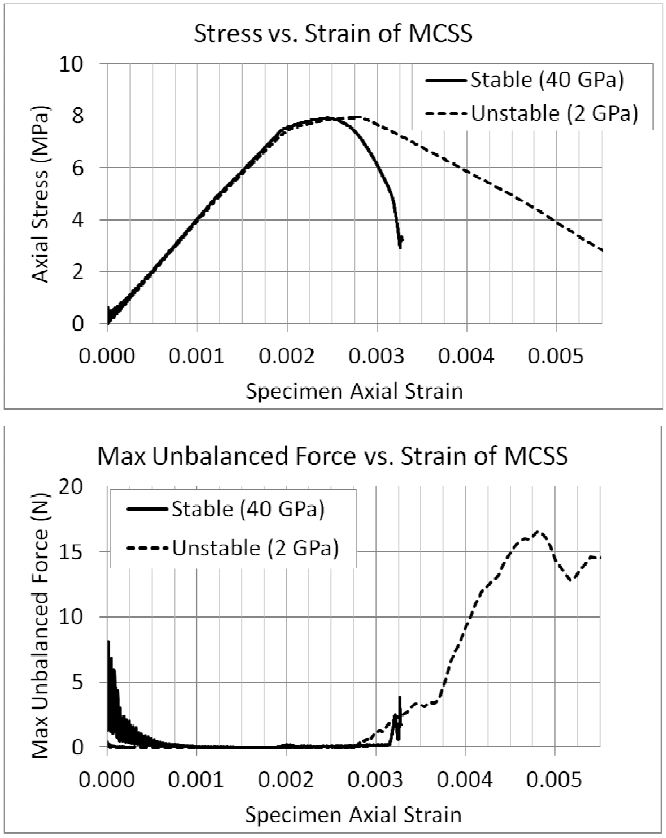

Fig. 3. Stress vs. strain of Mohr-Coulomb strain-softening specimen during stable (40 GPa platens) and unstable (2 GPa platens) failures with corresponding histories of maximum unbalanced forces.

Low platen stiffnesses such as the 2 GPa case elicited an unstable failure response in the specimen as indicated by the stress-strain response and by the maximum unbalanced force in the specimen. These unbalanced forces were carried through the model to additionally cause large accelerations, velocities, and shear strain rates during unstable failure conditions.

Identifier values were recorded only after the vertical specimen strain reached 0.001 in order to isolate the identifiers associated exclusively with the failure of the specimen. The unbalanced forces were large for high platen stiffnesses during initial loading, as can be seen in Figure 3.

The maximum values for the previously selected indicators were compared between the MC and the MCSS test cases to attempt to further isolate the unstable failure phenomenon from dynamic effects caused exclusively by changes to the loading system stiffness. The results from these tests are shown in semi-log plots in Figures 4 through 7.

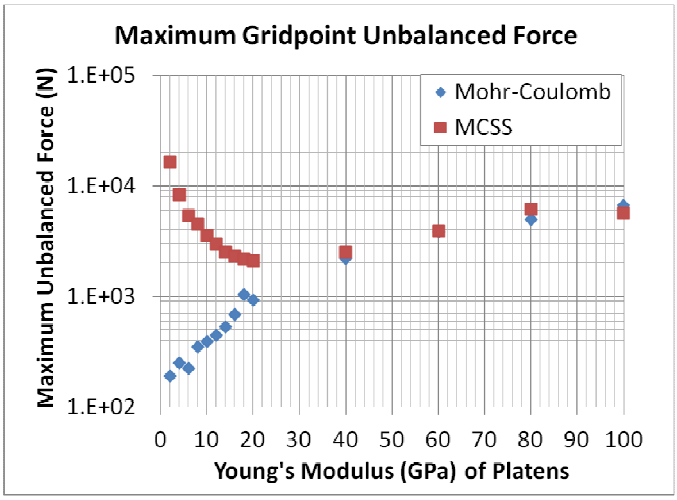

Fig. 4. Maximum gridpoint unbalanced force within specimen over a range of platen stiffnesses for both plastic Mohr-Coulomb and brittle Mohr-Coulomb strain-softening models.

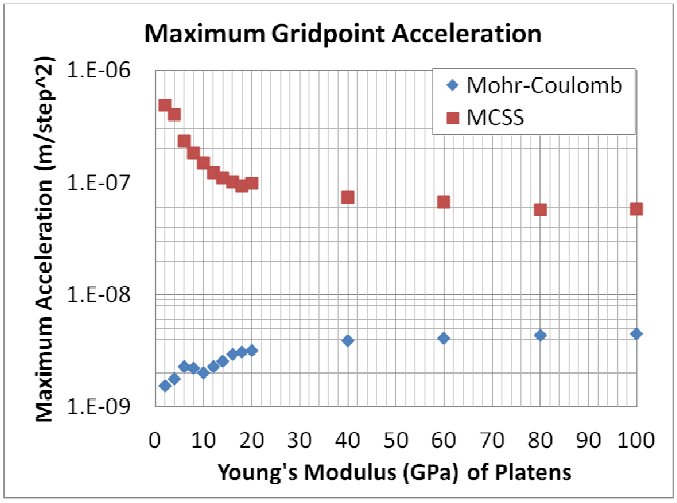

Fig. 5. Maximum gridpoint accelerations within specimen over range of platen stiffnesses for plastic Mohr-Coulomb and brittle Mohr-Coulomb strain-softening models.

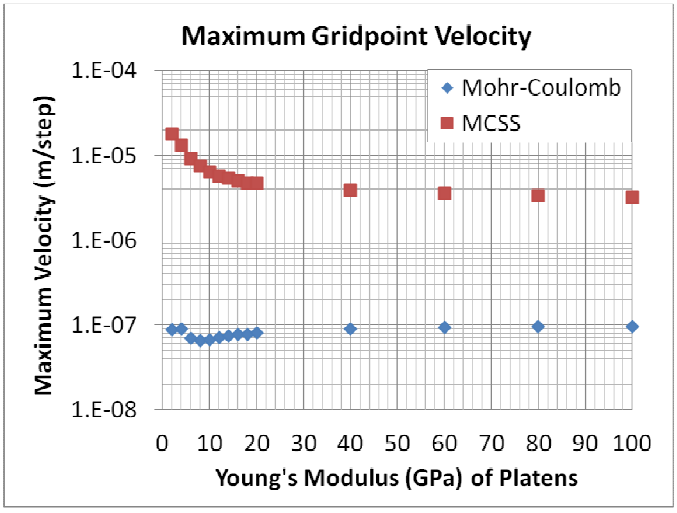

Fig. 6. Maximum gridpoint velocity within specimen over range of platen stiffnesses for plastic Mohr-Coulomb and brittle Mohr-Coulomb strain-softening models.

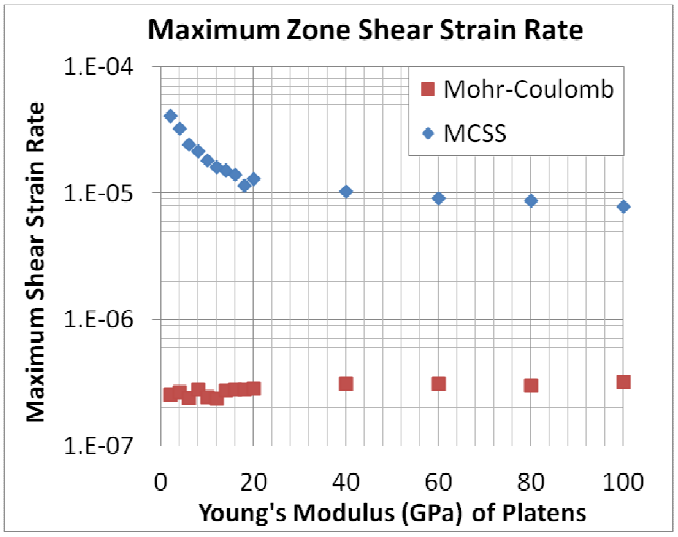

Fig. 7. Maximum zone shear strain rate within specimen over range of platen stiffnesses for plastic Mohr-Coulomb and brittle Mohr-Coulomb strain-softening models.

Note that the behavior of the indicators diverge between the MCSS and the MC cases with platen stiffnesses less than approximately 16 GPa. This change in behavior corresponded well with other measures of unstable failure and the previously assumed initiation of unstable failure for platens softer than the steepest portion of the specimen's stress strain response, which was approximately -20 GPa. By using the selected identifiers of instability, it was possible to directly distinguish between stable and unstable failures in the quasi-static model.

3. TRIAXIAL COMPRESSIVE STRENGTH TESTS

Further tests were conducted to determine the adequacy of using the selected unstable failure identifiers in FLAC3D under confined loading conditions. The confined tests were conducted on the previously calibrated brittle coal specimen. Confining pressures of 1 MPa to 6 MPa were applied to the specimen. It was found that the specimen assumed a friction angle of 30° and cohesion of 2.3 MPa during these confined tests. Stable failures were induced using stiff 100 GPa platens and unstable failures were induced using soft 2 GPa platens. The stress-strain results of the confined tests are shown in Figure 8 with stable and unstable results marked accordingly

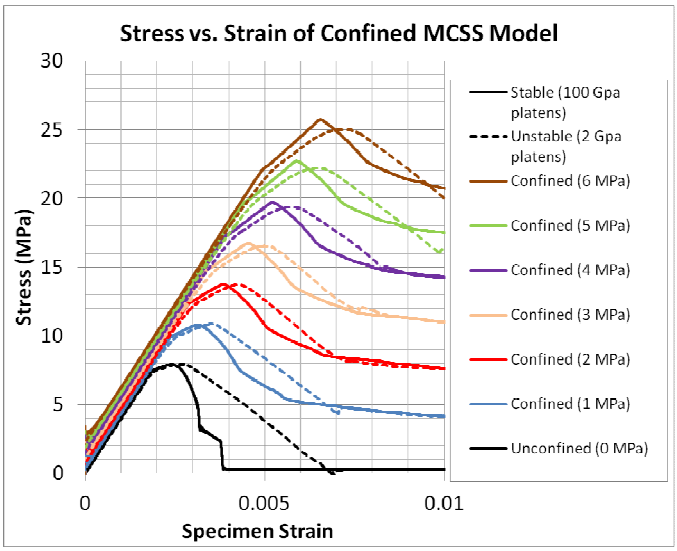

Fig. 8. Stress-strain responses of triaxially confined brittle coal specimens undergoing failure under unstable (2 GPa) and stable (100 GPa) platen loading conditions.

The specimen was found to assume a brittle yet hardening stress-strain behavior for increasing levels of confinement when a stiff, stable loading system of 100 GPa platens was applied to fail the specimen. The post-peak slope assumed the stiffness of the soft 2 GPa platens for the unstable failure cases.

3.1. Identifying Unstable Failures in Confined Specimen

Numerical identifiers were applied to determine the location, duration, and magnitude of unstable failure during the confined tests. The maximum unbalanced force recorded during the test was compared between a stable and unstable test case under 3 MPa of confinement. The results from this trial are shown in Figure 9.

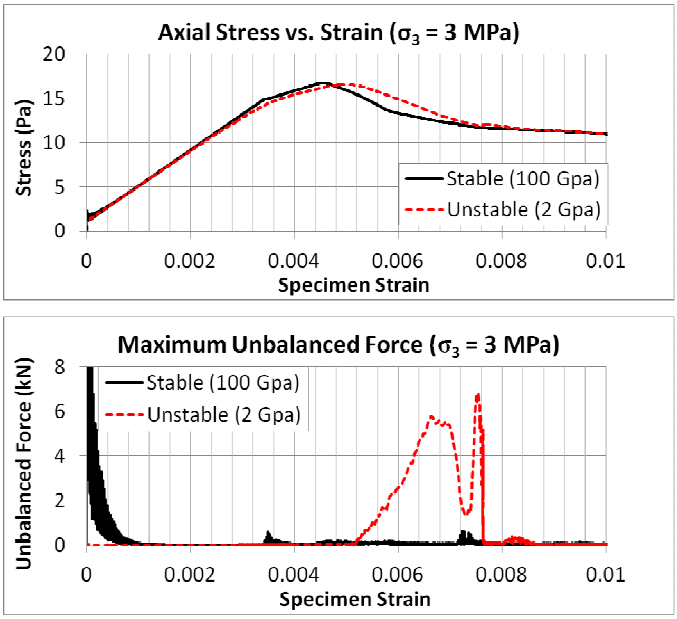

Fig. 9. Stress-strain and max unbalanced force in 3 MPa confined specimen under 100 GPa and 2 GPa loading.

The time history of the maximum unbalanced force shows large unbalanced forces as the specimen lost stability during the unstable 2 GPa platen loading case. Large unbalanced forces were not observed past initial loading during the stable failure using 100 GPa platens.

The indicators of unstable failure which were previously proposed were extended to the triaxial compressive strength tests. The results for the maximum indicator values within the specimen were recorded for each test and are shown in Figures 10(a-d). The maximum unbalanced force and acceleration were not calculated for the gridpoints located on the perimeter of the specimen during these confined tests due to numerical effects from the applied pressure boundary at these points. The velocity measurements were unaffected by the applied boundary and included a record of gridpoints at the perimeter of the specimen during the confined tests. The Mohr-Coulomb results from these trials have been included to provide a reference for how a fully stable, plastic model responded to changing platen stiffnesses and confinements as compared to the brittle Mohr-Coulomb strain-softening model which underwent unstable failure when the soft 2 GPa platens were used.

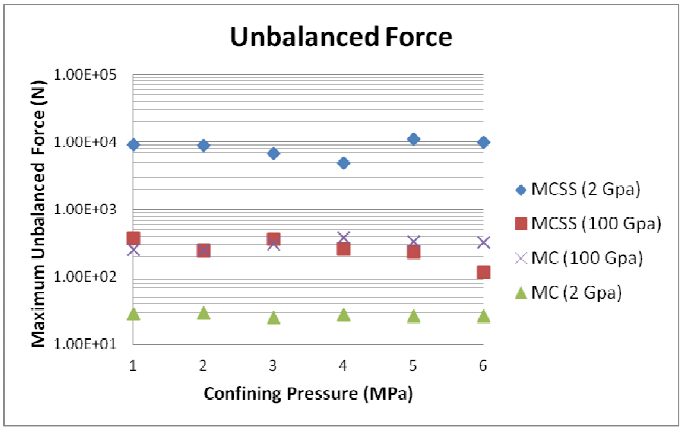

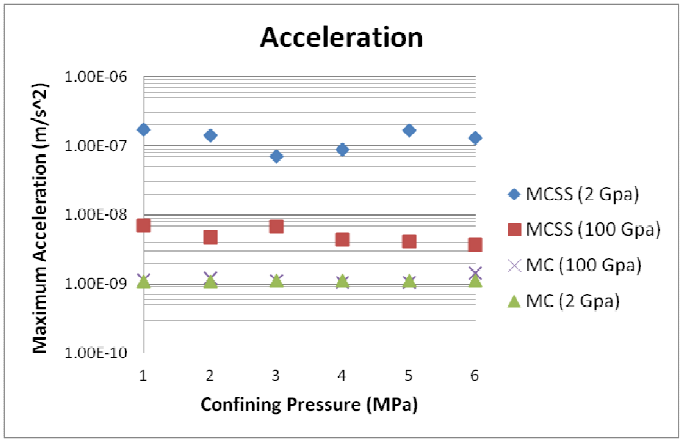

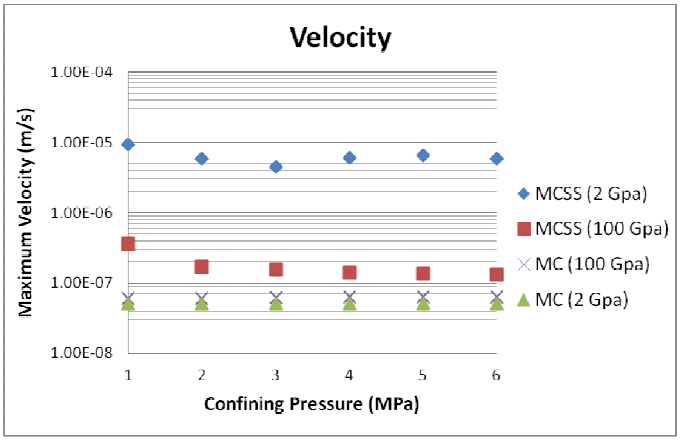

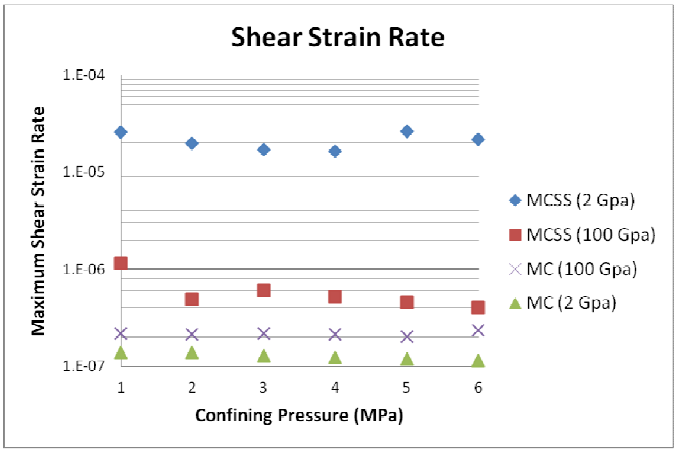

Fig. 10. Identifiers of stable vs. unstable failure for Mohr-Coulomb Strain Softening (MCSS) and Mohr-Coulomb specimens from 1 to 6 MPa confinement. a) Maximum unbalanced force at gridpoint. b) Maximum acceleration at gridpoint. c) Maximum velocity at gridpoint. d) Maximum zone shear strain rate.

The maximum values for the indicators of unstable failure show clear distinction in the magnitudes between stable and unstable test cases. Large unbalanced forces were observed at all levels of confinement for the soft loading condition as compared to the stiff, stable case at the same level of confinement. Large unbalanced forces then led to increased accelerations, velocities, and shear strain rates in the model. The effect of physical instability in the specimen could be separated from direct changes to the loading system stiffness by comparing the MCSS results to the MC results, which actually showed the opposite trend for dynamic effects in that the magnitudes of the indicators were higher for the stiffer 100 GPa platen case than the softer 2 GPa platen case.

The results of these tests showed good agreement with the uniaxial compressive strength tests. The selected identifiers of unstable failure all showed a trend of significantly increasing in magnitude during unstable failure.

4. CONCLUSIONS

Unstable failure was initiated within a series of FLAC3D explicit finite difference simulations using a comparatively soft loading system to fail a representative brittle coal specimen. Records of rapid dynamic motion were used to identify instability within the simulated coal specimen. Maximum unbalanced forces, accelerations, velocities, and shear strain rates were all found to correlate well with the onset of unstable failure, as confirmed through the stress-strain behavior of the specimen. These tests were repeated under uniaxial and triaxial confinement conditions, and compared against a perfectly plastic Mohr-Coulomb coal specimen under identical loading. It was found that an analysis of the proposed instability identifiers led to a clear distinction between stable and unstable failure results.

The continuum model in FLAC3D provided a useful tool for assessing the likelihood and magnitude of unstable failure assuming a pre-defined brittle response for a calibrated rockmass. Small magnitude unstable failures may also be assessed using this method.

By using the proposed identifier measures as a generic search function for finding and studying instability within these models, it is possible to extend these studies of unstable failure to include a range of complex geometries and loading configurations. Additional analyses should be conducted using more realistic material behaviors and geometries for the loading system to mimic in situ mining conditions. The results from these tests may provide valuable insight into reducing the real threat posed by rockbursts and coal bumps.

5. ACKNOWLEDGEMENTS

The work presented in this publication is part of an ongoing research activity conducted at the Colorado School of Mines which has been funded by the National Institute of Occupational Safety and Health (NIOSH). The contents of this publication are solely the responsibility of the authors and do not necessarily represent the official views of NIOSH.

REFERENCES

1. Salamon, M.D.G. 1970. *Int. J. Rock Mech. Min. Sci.* 7: 613-631. Great Britain: Pergamon Press.
2. Petukhov, I.M. and A.M. Linkov. 1979. *Int. J. Rock Mech. Min. Sci. & Geomech. Abstr.* 16: 57-76. Great Britain: Pergamon Press Ltd.
3. Iannacchione, A.T. and J. Zelanko. 1995. Occurrence and remediation of coal mine bumps: a historical review. In *Proceedings of the Mechanics and Mitigation of Violent Failure in Coal and Hard-Rock Mines, U.S. Bureau of Mines Special Publication 01-95*, 27-68.
4. Zubelewicz, A. and Z. Mróz. 1983. Numerical simulation of rock burst processes treated as problems of dynamics instability. *Rock Mechanics and Rock Engineering*. 16: 4, 253-274.
5. Larson, M.K. and J.K. Whyatt. 2009. Critical review of numerical stress analysis tools for deep coal longwall panels under strong strata. In *SME Annual Meeting and Exhibit*, *Denver, CO, 22-25 February 2009,* preprint 09-011. Littleton, CO: Society for Mining, Metallurgy, and Exploration, Inc.
6. Itasca Consulting Group Inc. 2010. *FLAC3D (Fast Lagrangian Analysis of Continua in 3 Dimensions), Version 4.0*. Minneapolis, MN:Itasca Consulting Group, Inc.
7. Kias, E.M.C., R. Gu, R. Garvey, and U. Ozbay. 2011 Modeling unstable rock failure during a uniaxial compressive strength test. In *Proceedings of 45th U.S. Rock Mechanics/Geomechanics Symposium, San Francisco, CA, 26-29 June 2011,* eds. A. Iannacchione et al, 825-833. Red Hook:Curran Associates, Inc.